Journal of Nuclear Materials 408 (2011) 129–135

Contents lists available at ScienceDirect

Journal of Nuclear Materials

journal homepage: www.elsevier.com/locate/jnucmat

Chemically produced nanostructured ODS–lanthanum oxide–tungsten composites sintered by spark plasma

Mazher Ahmed Yar [a,*], Sverker Wahlberg [b], Hans Bergqvist [b], Hanadi G. Salem [c], Mats Johnsson [d], Mamoun Muhammed [a,*]

[a] Division of Functional Materials-ICT, Sweden
[b] Royal Institute of Technology (KTH), Stockholm 164 40, Sweden
[c] Department of Mechanical Engineering, American University in Cairo, Egypt
[d] Department of Materials and Environmental Chemistry, Stockholm University, Stockholm, Sweden

ARTICLE INFO

Article history:
Received 3 August 2010
Accepted 27 October 2010

ABSTRACT

High purity W and W–0.9La_2O_3 (wt.%) nanopowders were produced by a wet chemical route. The precursor was prepared by the reaction of ammonium paratungstate (APT) with lanthanum salt in aqueous solutions. High resolution electron microscopy investigations revealed that the tungstate particles were coated with oxide precipitates. The precursor powder was reduced to tungsten metal with dispersed lanthanum oxide. Powders were consolidated by spark plasma sintering (SPS) at 1300 and 1400 °C to suppress grain growth during sintering. The final grain size relates to the SPS conditions, i.e. temperature and heating rate, regardless of the starting powder particle size. Scanning electron microscopy revealed that oxide phases were mainly accumulated at grain boundaries while the tungsten matrix constituted of nanosized sub-grains. The transmission electron microscopy revealed that the tungsten grains consist of micron-scale grains and finer sub-grains. EDX analysis confirmed the presence of W in dispersed oxide phases with varying chemical composition, which evidenced the presence of complex oxide phases (W–O–La) in the sintered metals.

1. Introduction

Tungsten is an important and prominent metal among the refractory metals due to an excellent combination of outstanding high temperature properties and high melting point (highest of all metals). Its high strength and corrosion resistance at elevated temperatures, good thermal conductivity and low thermal expansion makes it possible to use tungsten in high temperature applications. On the other hand, owing to its high hardness and wear resistance, high modulus of elasticity and compression strength, tungsten is an important constituent as an alloying element in tool steel, superalloys, stellites and hard metal industry [1].

Besides the above properties, tungsten is a low-activating metal with a low sputtering yield in radiation environment [2] and is supposed to be the most promising candidate for plasma facing wall material in future fusion reactors. Recent studies on plasma–wall interaction, demand a material to withstand the extreme conditions (high temperatures and radiation environment i.e. electrons, protons, neutrons and α-particles). In modern fusion reactor design, an armor material must have high melting point and stable mechanical properties at elevated temperatures (strength, creep, fatigue etc.), high thermal conductivity, low coefficient of thermal expansion and thermal shock resistance, reduced activation and high sputtering resistance [1–5]. To bear up the thermal conditions, carbon–carbon composites are good heat conductors but the higher erosion rates and low sputtering resistance make it unacceptable for high quality and stable plasma reaction. The rate of materials erosion determines both the service lifetime of components and the quality of the plasma. So far, only tungsten or its alloys seem to be a better choice for longer and smooth running of high quality plasma as well as for economy and efficiency of a commercial fusion reactor [1–5].

Tungsten materials, however, are facing serious challenge of brittleness in different aspects i.e. low-temperature brittleness, high-temperature or recrystallization brittleness and radiation induced brittleness [6]. Higher ductile-to-brittle transition temperature (DBTT) of pure tungsten and tungsten-based materials is the major obstacle during the processing and service. Most of the bulk tungsten metal is being produced by powder metallurgy methods. Due to very high melting point, its sintering is carried out at higher temperatures, usually followed by hot mechanical working to achieve a high density material, since relative density is a major

* Corresponding authors. Tel.: +46 8 790 8158; fax: +46 8 790 9072.
E-mail addresses: mayar@kth.se (M.A. Yar), sverker@kth.se (S. Wahlberg), hansber@kth.se (H. Bergqvist), hgsalem@aucegypt.edu (H.G. Salem), matsj@inorg.su.se (M. Johnsson), mamoun@kth.se (M. Muhammed).

0022-3115/$ - see front matter © 2010 Elsevier B.V. All rights reserved.
doi:10.1016/j.jnucmat.2010.10.060

factor which determines the mechanical properties of bulk tungsten [7,8]. Consequently, processing of tungsten involves prolonged exposure to higher temperatures resulting in grain growth, which reduces room-temperature mechanical properties by grain boundary weakening [7,9]. On the other hand, tungsten-based materials inherently exhibit low toughness and almost no ductility (bcc structure) so they cannot be employed for structural applications at temperatures lower than DBTT. Therefore, efforts have been directed to induce some plasticity and alloying addition has turned out to be an effective way to improve ductility by lowering the DBTT [7,10].

Recrystallization is another factor which deteriorates high temperature strength and creep resistance of tungsten and limits its deployment in extremely high temperature applications. These problems can be overcome by dispersion strengthening and precipitation hardening, Non-Sag tungsten [11,12] and W–ThO_2 (ODS–W) as examples. However, the radioactive nature of thorium has turned development efforts towards tungsten alloys strengthened by other metal oxides like La_2O_3, Y_2O_3, HfO_2, ZrO_2, CeO_2 [13–18]. Dispersed oxide particles inhibit recrystallization and grain growth as well as improving the high temperature strength and creep resistance by hindering grain boundary sliding [14–16]. Unsatisfactory results in the low-temperature range may be outcomes of coarse tungsten grains and/or micron sized dispersed particles or anisotropic non-homogeneous microstructure [19–21]. Ultrafine grained (UFG)/nanostructured tungsten alloys have showed better high temperature properties and also some ductility at lower temperatures as compared to coarse grained conventional materials [22]. In addition, nanostructured materials with high density of sinks (grain boundaries) were suggested as they exhibit higher irradiation resistance due to higher capacity to accumulate radiation induced defects and less integration of defects at grain boundaries [23–29]. It seems that nanostructuring of ODS–tungsten alloys could be the effective way to use them within the permissible temperature window and the radioactive environment of a fusion reactor.

Today most nanostructured ODS–tungsten materials are being prepared by mechanical milling. This method involves high energy consumption during prolonged milling processes and have serious drawbacks of less control over purity and detrimental contaminations from balls/container or milling medium, which adversely affect the material properties [8,30,31]. High amount of mechanical energy induced into the powder particles during milling can cause an accelerated grain growth and sometimes high internal stresses leading to cracking of the compacts during sintering [32]. These internal stresses may result in a premature failure of the component when superimposed by thermal stresses during service. To overcome these problems wet chemical processing comes with a solution to produce high purity nanocomposites. These methods (bottom-up approach) can fabricate complex nanostructured materials and have shown high potential to produce molecular engineered nanomaterials with exact composition at very high purity and homogeneity. These methods are also suited for the fabrication of tungsten based composites [33–37]. We have developed a novel method for the synthesis of nano ODS–W powders, in which a precursor of tungsten and metal oxides is prepared by the reaction of tungsten and lanthanum salts in aqueous solution at room temperature. The obtained precursor is highly homogenous where the two components are mixed at the molecular level. The precursor is then reduced at high temperature to nanosized tungsten grains with uniform distribution of lanthanum oxide. This method, besides being simple, it is also suitable for large scale production. The sintering of nanosized powders into dense bulk metal while preserving their nanoscale structure remains to be a challenge. When nanophase materials are exposed to high temperature for longer time, interfaces of nanoparticles usually diffuse rapidly to reduce the high surface energy resulting in a substantial grain growth with grains well above the nano-regime.

Spark plasma sintering (SPS) is a comparatively new technique and has been successfully applied for consolidation of cermets, ceramics, metals and alloys including refractory materials. SPS process allows the consolidation of powder materials into fine-grain and high density sinters at relatively low temperatures compared to e.g. hot-pressing. Samples are heated in a more efficient way in the spark plasma sintering process compared to in most conventional sintering techniques. The powder is loaded in electrically and thermally conductive graphite dies, where a DC current is applied in pulses from the beginning to the end of sintering cycle under a uniaxial pressure. When current passes through the dies, and also the sample (in some cases), the sample is heated both from outside (dies act as heating element) and inside (due to electrical resistance of material). Thus very fast heating (up to 1000 °C min^{-1}) and cooling rates, short holding times (minutes) make SPS a unique sintering process as compared to hot pressing (50–80 °C min^{-1}) [38]. SPS process makes it possible to achieve fully dense material at relatively lower temperatures, typically a few hundred degrees lower than in normal hot pressing [39]. Three main factors are considered responsible for rapid densification: (i) very high heating and cooling rates; (ii) high mechanical pressure applied during the process; and (iii) the use of pulsed DC current [40]. The SPS technique can therefore prove better than conventional sintering methods for consolidation of tungsten powders. In this work the idea was to merge the novel wet chemical method and SPS process to achieve a final nanostructured tungsten material with improved quality (purity) and properties.

Accordingly, in the current research, tungsten powder doped by means of wet chemistry methods has been employed for the production of W–ODS composites by utilizing SPS technique for consolidation. Characterization of the doped powders before and after sintering was conducted.

2. Experimental

2.1. Precursor synthesis, reduction and sintering

Lanthanum doped tungsten precursors with lanthanum content corresponding to W–0.9 wt.% La_2O_3, were synthesized from ammonium paratungstate, $(NH_4)_{10}[H_2W_{12}O_{42}]\cdot 4H_2O$ (APT) and lanthanum nitrate hydrate, $La(NO_3)_3\cdot xH_2O$ (Aldrich). 50 g of as-received APT powder and 0.86 g of lanthanum nitrate hydrate were added in 153 mL of water. The reaction was carried out under stirring at room temperature. The solution was filtered after 24 h reaction (sufficient time to ensure complete reaction between APT and La ions) and the obtained powder was dried at room temperature. A sample from obtained dried powder was used for chemical analysis and was found to contain 69 wt.% W and 0.5 wt.% La. The precursor was calcined followed by reduction in a tube furnace. The calcination was carried out under nitrogen atmosphere at 450 °C for 1 h whereby the powder is transformed into oxide mixture. The reduction was done by heating under pure hydrogen atmosphere at 800 °C for 6 h. The heating rate up to the processing temperatures was 5 °C/min. In a separate experiment, the as-received APT was reduced to pure tungsten powder under the same conditions. In another set of experiments, the reduction was carried out in two steps; first at 600 °C for 2 h, then the temperature was raised to 800 °C and the reduction was allowed to proceed for 6 h. All samples were cooled overnight under a hydrogen flow.

The spark plasma sintering was carried out using Dr. Sinter 2050 SPS (Sumitomo Coal Mining Co., Japan) sinter reduced powders under vacuum using graphite dies. Powders were sintered at two different temperatures (1300 and 1400 °C) under 75 MPa

pressure, for 3 min. Densities of sintered samples were measured. The relative densities (RD) were calculated using theoretical densities of tungsten and La_2O_3 as 19.25 g cm^{-3} and 6.57 g cm^{-3} respectively [41,42]. Polished sintered samples were subjected to Vickers microhardness testing under 200 g load and a dwell time of 20 s at room temperature.

2.2. Microstructural characterization

Both powders and sintered samples were subjected to microstructural characterization using analytical high resolution field emission scanning (HRSEM) and transmission electron microscopes (HRTEM). High resolution scanning electron microscope (Gemini, Zeiss-Ultra 55) equipped with high resolution In-lens secondary, backscattered electron (ESB) detectors and "INCA Energy" energy dispersive X-ray (EDX) analytical system, was used for elemental analysis. Grain sizes were measured from SE images of fractured samples. TEM sample was prepared in a "FEI-Quanta 3D" focused ion beam-scanning electron microscope (FIB-SEM) using 30 kV Ga ion beam. Final polishing was done using 5 and 2 kV ion beams to remove amorphous layer. HR-STEM (JEOL, JEM-2100F) was used for characterization of sintered samples and elemental analysis of different phases using EDX detector.

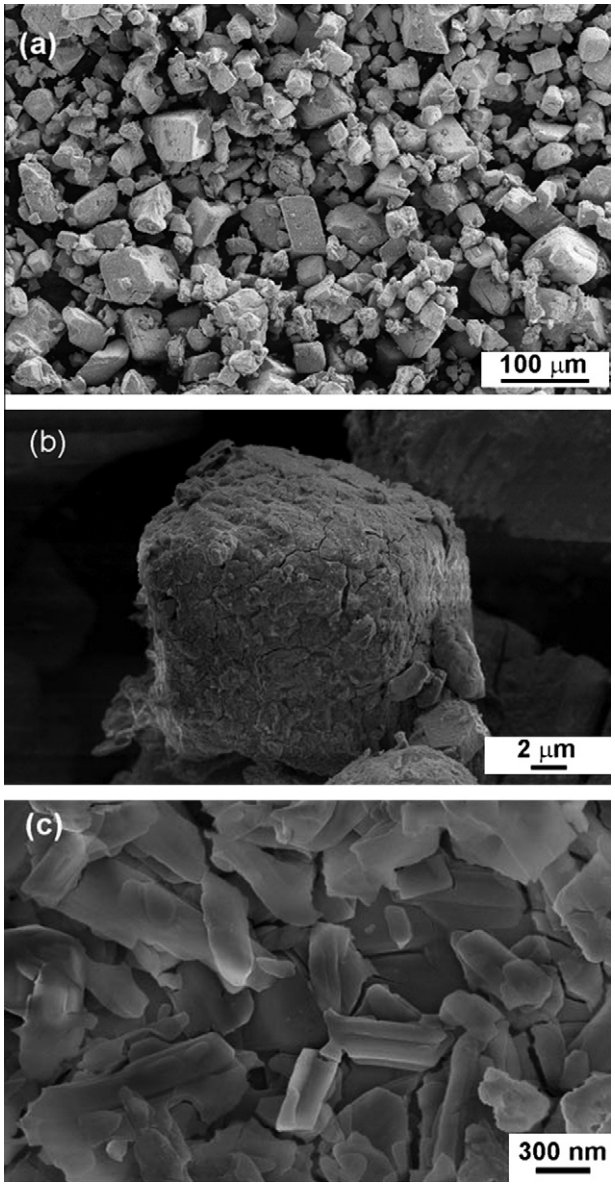

Fig. 1. SEM micrographs showing (a) precursor powder, (b) coated APT shaped particle, and (c) HR-magnified image of coated particle surface.

3. Results and discussion

3.1. Synthesized W–La_2O_3 precursor

The synthesized powder precursors were analyzed in high resolution scanning electron microscope (HRSEM). La doped-W precursor powder was rather similar to starting APT powder in morphology, with very wide particle size distribution (10–70 μm), as shown in Fig. 1a. As revealed from HRSEM analysis, La containing oxide products were found on the surface of the APT particles, (Fig. 1b and c). Since the shape of particles was same as starting APT particles (which has limited solubility in aqueous solution) it

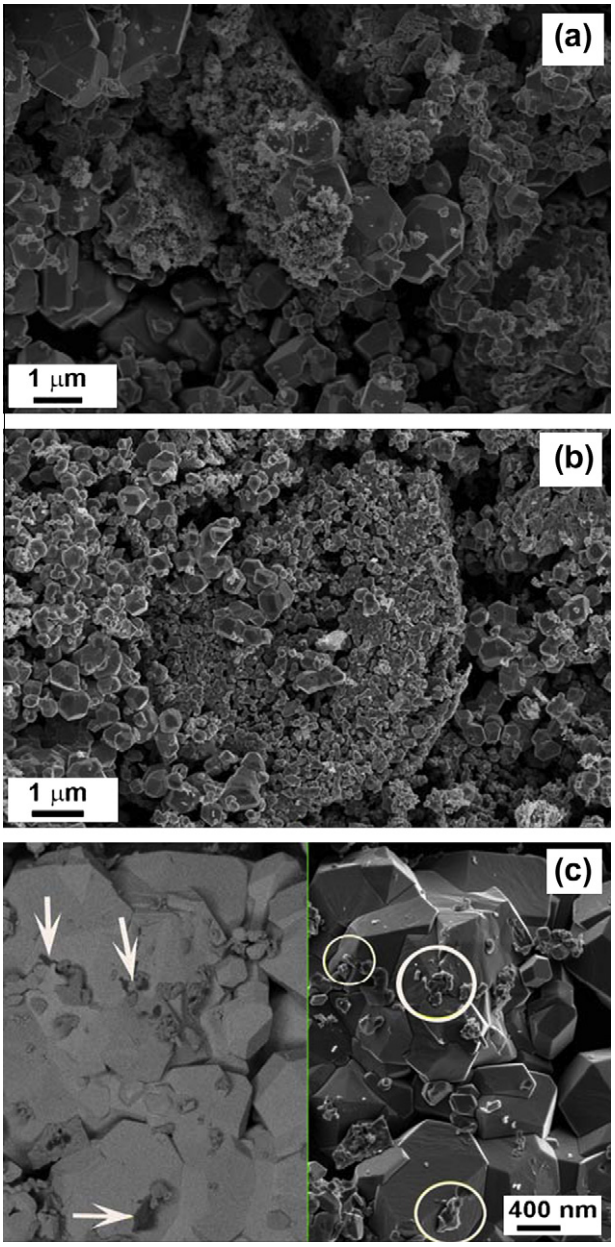

Fig. 2. SEM micrograph of (a) powder reduced in one step at 800 °C, (b) nanogranular tungsten in APT pseudomorphs, (c) In-lens ESB image (left half) showing oxide nanoparticles indicated by arrows and similar sites circled on the right half of the SE image.

can be assumed that the reaction takes place at the surfaces of APT particles nanosized particles were also observed in precursor.

3.2. Reduced powder

Reduction of APT and APT-La synthesized precursors in one step at 800 °C (samples 1 and 2) produced loosely agglomerated powders with tungsten grains of submicron to micron size (Fig. 2a). Reduction of the precursor in two steps (sample 3), resulted in submicron tungsten grains and nanocrystalline tungsten sponges in APT pseudomorphs (Fig. 2b). La-oxide nanoparticles were revealed on the surface of tungsten grains. Left half of Fig. 2c is an In-lens backscattered electron image (Z-contrast) showing dark grey oxide nanoparticles (pointed by arrows) while right half is the corresponding In-lens secondary image from the same area showing nanoparticles (encircled) on the surface of tungsten grains. Qualitatively La and oxygen were confirmed in these nanoparticles by energy dispersive X-ray (EDX) analysis at 20 kV. Tungsten was also detected together with La and oxygen, due to comparatively a large interaction volume in relation to grain size.

3.3. Powder sintering via SPS

Powder samples were sintered into compacts of 12 mm in diameter and around 2.5 mm in height. Final sintering temperatures (T_F) and heating rates were changed while pressure and holding time were set constant in SPS process. Sintering parameters for different samples are given in Table 1.

Table 1
Sintering conditions, density, grain size and H_V for different compacted alloys, (holding time 3 min at T_F), pressure 75 MPa.

Sample ID	Composition (wt.%)	Heating rate (°C/min)	T_F (°C)[a]	Density (g/cm^3)/(%RD)[b]	Grain size (μm)	H_{V200g} (±10)
1	Pure W	100	1300	17.3/91	3.0	317
2	W-0.9La_2O_3	100	1300	16.9/89	4.2	327
3	W-0.9La_2O_3	50	1400	17.8/94	9.7	406

[a] Plateau temperature.
[b] Relative density.

The grain size measurements reveal dependence on the sintering temperature and heating rate rather than the particle size of the starting powders (Fig. 3). Pure tungsten sample sintered at 1300 °C for 3 min and at 75 MPa pressure resulted in a bulk material with a density of 17.3 g cm^{-3} (relative density 91%). It is clear that SPS produced consolidated material with much higher density and hardness values at lower sintering temperature when compared with the earlier reported results for conventional sintering of mechanically mixed tungsten based powders (for instance Kim et al. [43]). Table 1 compares the Vickers microhardness number (VHN) measured for the pure W and ODS–W samples. Comparing samples 1 and 2, we notice an increase of the hardness in spite of the noticeable decrease of the density. This can be attributed to the strengthening by the oxides. It is suggested that the oxide dispersion in the W-powders hindered diffusion at some of the interfaces, which explains the higher measured density for the pure W.

On the other hand, comparing samples 2 and 3, it is seen that the hardness increases with the density. The higher relative density was displayed for the ODS–W compact sintered at higher temperature (sample 3), which should have enhanced diffusion and hence higher hardness value. It is worth noting that density and dispersion strengthening were the dominating factors that influenced the hardness of ODS–W and the post sintering grain size did not have a significant effect. It is also worth noting that although the initial powder crystallite size of sample 3 is finer than that of sample 2, increasing the sintering temperature to 1400 °C resulted in grain coarsening to 9.7 μm. It is suggested that accelerated grain growth in sample 3 is also due to the finer crystallite size of powder which obviously have a higher tendency for grain growth. Not much work has been reported in earlier published literature on spark plasma sintering of ODS–W composites. Kim and his group [44], have studied the consolidation of mechanically milled tungsten composites containing La_2O_3 by SPS process. In their study they used higher sintering temperature 1700 °C, and they obtained slightly higher density and hardness as compared to sample 3 which was sintered at much lower temperature (1400 °C).

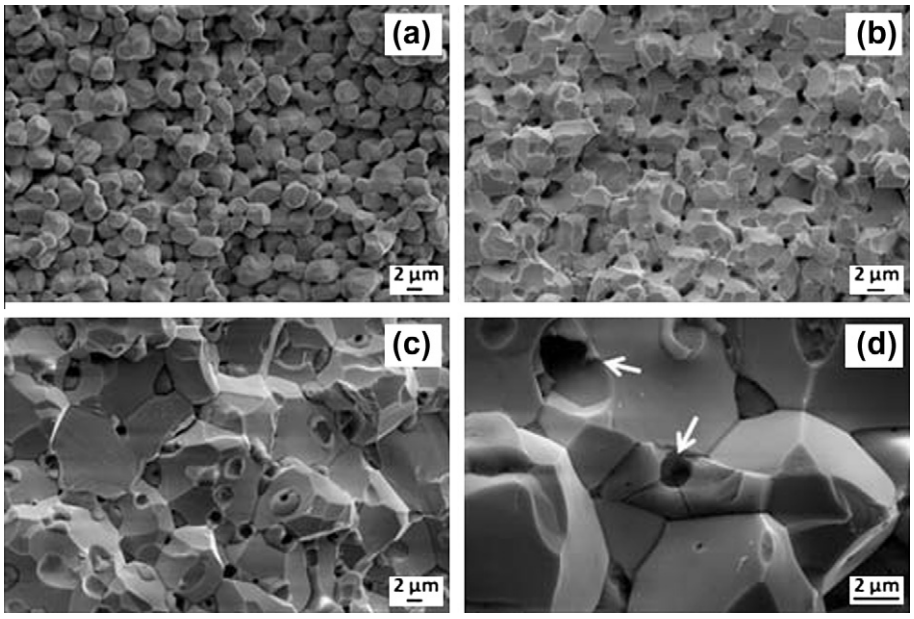

Fig. 3. SEM micrographs of samples sintered at (a) 1300 °C, pure W, (b) 1300 °C, W-0.9% La_2O_3, (c) 1400 °C, W-0.9% La_2O_3, and (d) sample 3 at higher magnification showing blown up gas bubbles surrounded by oxides.

Fractured surfaces of the sintered samples revealed porosity in all samples at the grain boundaries and at triple junctions between tungsten grains. In the ODS–W samples, most of the porosity was filled by second phase. Samples sintered at 1400 °C showed less porosity as compared to those sintered at 1300 °C (Fig. 3), which supports the discussion made in the previous paragraph. Fig. 4a shows the distribution of dispersed oxides in the sintered samples. Dark grey areas represent La containing phase. Channeling contrast from the backscattered electron detector revealed sub-grains in the tungsten matrix (Fig. 4b). The origin of these sub-grains is nano tungsten crystals comprising different orientations in APT pseudomorphs in reduced powder. During the SPS processing nanocrystals sintered together and diffused into each other under high pressure and temperature. Most of the sub-grain boundaries were free from oxides, which evidenced that oxides are not doped into the APT particles during solution treatment.

Both fractured and polished samples were subjected to EDX point analysis in SEM to analyze the composition of tungsten and oxide phases. EDX analysis revealed that the second phase present at grain boundaries is a new mixed oxide of La and W, and determined relative densities may not be accurate. These mixed oxide phases could be a reason for the slightly coarser grain size of ODS sample as compared to pure tungsten. Such mixed phases have also been reported by other groups [31,44,45].

The composition of the oxide phase was determined by EDX using La_2O_3 standard. Normalized EDX results from different oxide grains in polished samples are given in Table 2. Sample 3 sintered at 1400 °C showed oxide phases with blown up spherical microporosities/gas bubbles (Fig. 3d). It is suggested that the source of such gases could be the result of incipient melting of the new oxides during the spark plasma sintering. The entrapped gases expand on heating during the sintering. During the cooling stage, after the sintering cycle, the high circumferential pressure imposed by the contracting metal grains may have resulted in blowing up of gas bubbles leaving behind a cracked oxide layer (pointed at by arrow in Fig. 3d). However, further investigation is required to understand this phenomenon.

Table 2
Elemental composition of oxides phases in sample 2 (At.%, normalized).

	O	La	W
Average	67.9	14.8	17.2
Std. dev.	0.4	0.3	0.4

The W–La_2O_3 bulk sample sintered at 1300 °C was investigated by TEM after specimen preparation using focused ion beam (FIB). The TEM sample had few tungsten and oxide grains. Selected area diffraction (SAD) patterns from tungsten grains were identified as cubic α-tungsten with a lattice parameter of 3.16 Å. Only a few tungsten grains were found with sub-grain boundaries, as shown in Fig. 5. High resolution imaging and SAD from one sub-boundary revealed low angle boundaries; such an image is shown in Fig. 5b. Low angle boundaries may be helpful for improving the ductility of bulk material since they are coherent with the matrix [46].

Dislocation lines and loops were also observed in tungsten grains, as shown in Figs. 5a and 6c. Beside these features, areas with dislocation activity were also observed. Fig. 6a and b depicts high resolution images from an area with dislocations. These dislocations were similar to those observed in highly deformed

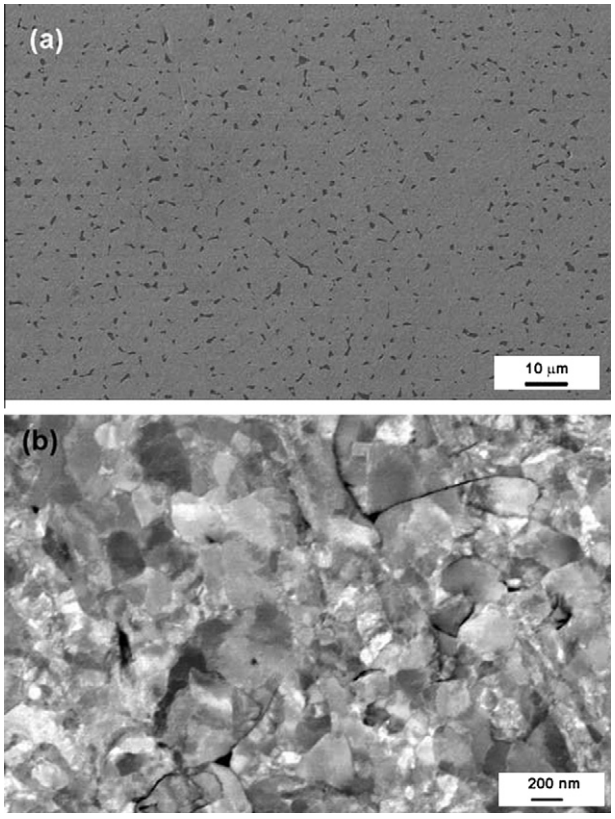

Fig. 4. (a) SE micrograph of sintered sample at 1400 °C, and (b) BSE-channeling contrast showing nanosized sub-grains.

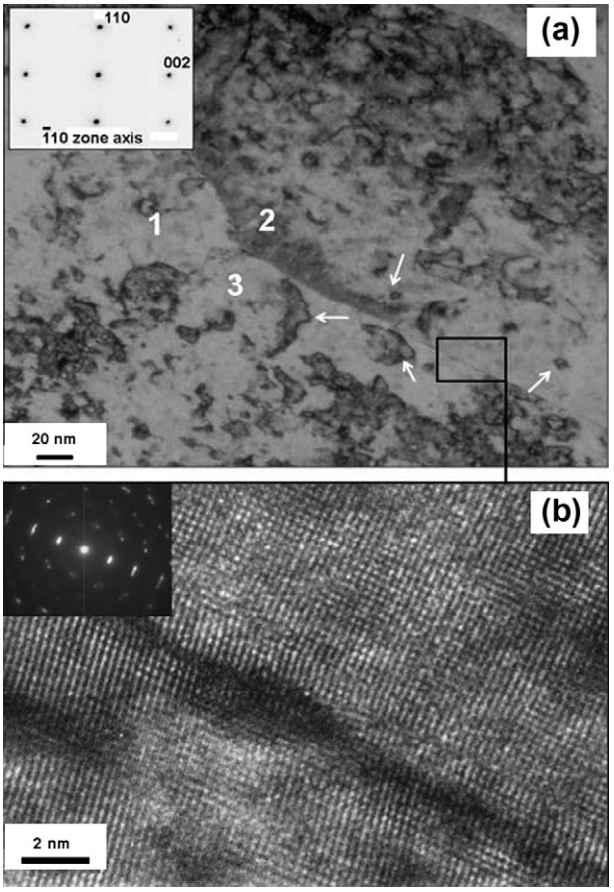

Fig. 5. TEM images showing (a) tungsten grain with sub-grains (1, 2 and 3) and loop/line dislocations pointed by white arrows, inset; SAD pattern of tungsten along [−1 1 0] zone axis, and (b) HR image showing low angle sub-boundaries and SAD pattern from sub-grains 1, 2 and 3 (inset).

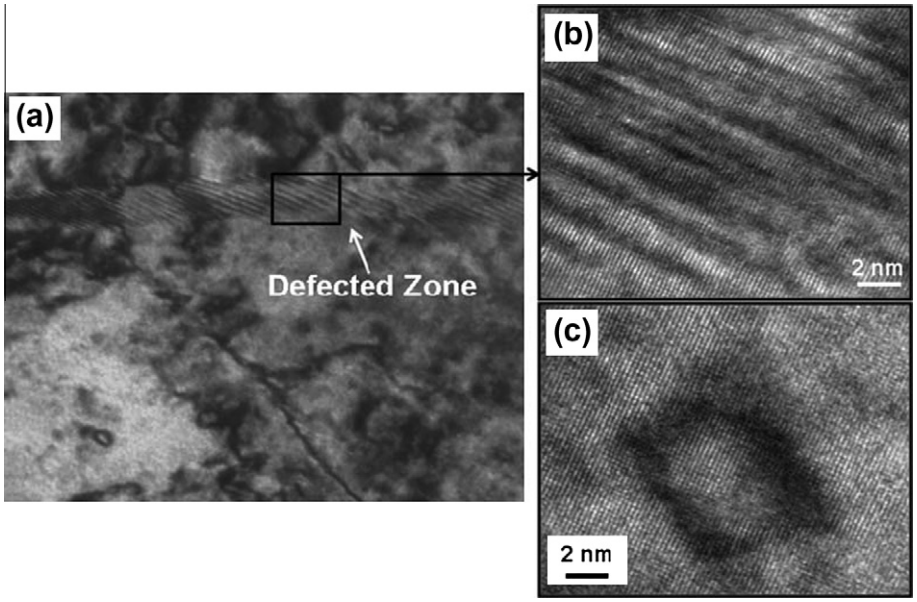

Fig. 6. TEM images showing tungsten grain with dislocation activities (a) and (b), HR image of a dislocation loop (c).

materials, which indicate that powder particles undergo deformation under the high pressure associated with the SPS process. Apparently a high density of dislocation lines and loops were observed. Primary reason for these growth defects is very short holding time at higher temperatures (in the order of minutes) and enough time was not available to attain a thermal equilibrium to diminish these dislocations.

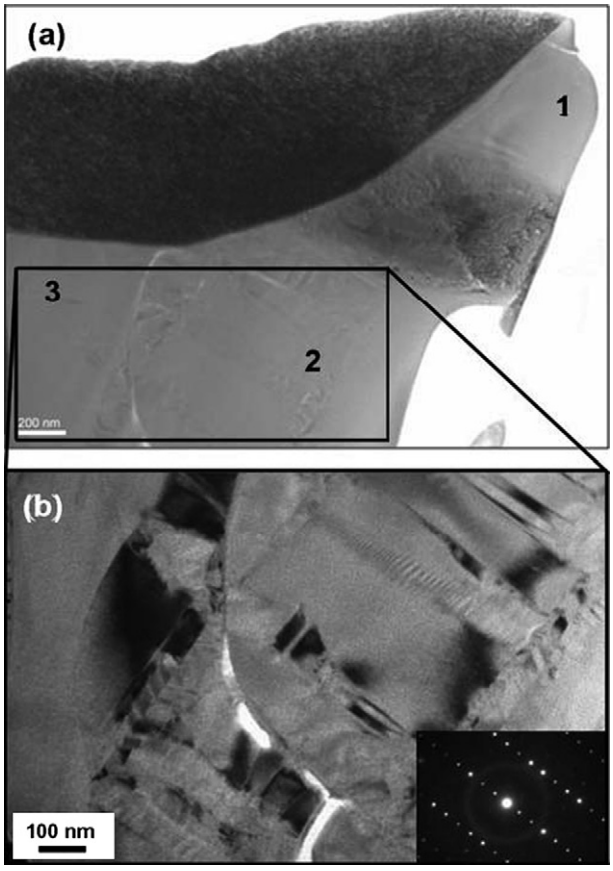

Fig. 7. (a) Overview of analysed oxide grains in TEM, and (b) high contrast image showing sub-grain features in oxide phase, inset; SAD of oxide phase.

Observations made by TEM on oxides revealed sub-grain features as shown in high contrast images, as shown in Fig. 7b. EDX analysis was carried out in STEM mode with 0.5 nm electron beam spot size from different oxide grains and the presence of tungsten together with La and oxygen was confirmed. Elemental analysis showed different results from one grain to another and within a single oxide grain. The chemical composition and SAD patterns of these oxides do not agree with previously reported W–La oxides in the literature. SAD patterns from these oxides showed ring indicating an amorphous structure, while the high resolution imaging has also confirmed the presence of amorphous material together with crystalline phases. It is difficult to explain the presence of this amorphous material. It is possible that it was induced by the ion beam during specimen preparation, since no amorphous material was observed in tungsten grains. The diffraction patterns are under investigation to identify these phases.

4. Conclusions

High purity nanocrystalline oxide dispersed-tungsten powders were successfully synthesized by controlled chemical reactions from aqueous solution at room temperature for 24 h. The particles of the precursor powders were coated with La-containing products on the surface, rather than doped inside. This implies that distribution of oxide phase in bulk ODS metal is defined by APT particles size and its distribution in precursor powder. ODS–tungsten composites are successfully sintered by SPS technique at temperatures significantly lower than those in conventional sintering methods which avoided substantial grain growth. Tungsten matrix consists of micron sized grains having fine sub-grains with low angle boundaries. Hardness of sintered samples depends primarily on the degree of densification. Although, the higher sintering temperature (1400 °C) results in higher degree of densification and hence higher hardness, incipient melting of La–W–oxides occurs.

Acknowledgements

The work was partially financed by the European Fusion Development agreement (EFDA), the European FP7 Project FEMaS and The Swedish Research Council (VR). Authors of the work would like to acknowledge Dr. Mats Waldenström of Sandvik AB for providing

the APT samples and P.O. Söderholm, Department of Materials Science and Engineering, KTH for assistance with Vickers microhardness testing. M. A. Yar is grateful to Higher Education Commission (HEC), Govt. of Pakistan for financial support during his PhD studies.

References

[1] E. Lassner, W.-D. Schubert, Tungsten: Properties, Chemistry, Technology of the Element, Alloys, and Chemical Compounds, first ed., Kluwer Academic/Plenum Publishers, New York, 1999.
[2] P. Norajitra, L.V. Boccaccini, E. Diegele, V. Filatov, A. Gervash, R. Giniyatulin, S. Gordeev, V. Heinzel, G. Janeschitz, J. Konys, W. Krauss, R. Kruessmann, S. Malang, I. Mazul, A. Moeslang, C. Petersen, G. Reimann, M. Rieth, G. Rizzi, M. Rumyantsev, R. Ruprecht, V. Slobodtchouk, J. Nucl. Mater. 329–333 (2004) 1594–1598.
[3] E. Diegele, R. Krussmann, S. Malang, P. Norajitra, G. Rizzi, Fusion Eng. Des. 66–68 (2003) 383–387.
[4] G.A. Cottrell, Mater. Sci. Technol. 22 (8) (2006) 869–880.
[5] P. Norajitra, L.V. Boccaccini, A. Gervash, R. Giniyatulin, N. Holstein, T. Ihli, G. Janeschitz, W. Krauss, R. Kruessmann, V. Kuznetsov, A. Makhankov, I. Mazul, A. Moeslang, I. Ovchinnikov, M. Rieth, B. Zeep, J. Nucl. Mater. 367–370 (2007) 1416–1421.
[6] I. Smid, M. Akiba, G. Vieider, L. Plöchl, J. Nucl. Mater. 258–263 (1998) 160–172.
[7] Y. Kitsunai, H. Kurishita, H. Kayano, Y. Hiraoka, T. Igarashi, T. Takida, J. Nucl. Mater. 271–272 (1999) 423–428.
[8] Y. Ishijima, H. Kurishita, K. Yubuta, H. Arakawa, M. Hasegawa, Y. Hiraoka, T. Takida, K. Takebe, J. Nucl. Mater. 329–333 (2004) 775–779.
[9] A.V. Babak, Powder Metall. Met. Ceram. 22 (4) (1983) 316–318.
[10] Y. Mutoh, K. Ichikawa, K. Nagata, M. Takeuchi, J. Mater. Sci. 30 (1995) 770–775.
[11] J.W. Pugh, Metall. Trans. 4 (2) (1973) 533–538.
[12] P.K. Wright, Metall. Trans. A 9 (7) (1978) 955–963.
[13] J.W. Davis, V.R. Barabash, A. Makhankov, L. Plöchl, K.T. Slattery, J. Nucl. Mater. 258–263 (1998) 308–312.
[14] M. Mabuchi, K. Okamoto, N. Saito, M. Nakanishi, Y. Yamada, T. Igarashi, Mater. Sci. Eng. A 214 (1996) 174–176.
[15] M. Mabuchi, K. Okamoto, N. Saito, T. Asahina, T. Igarashi, Mater. Sci. Eng. A 237 (1997) 241–249.
[16] H.J. Ryu, S.H. Hong, Mater. Sci. Eng. A 363 (2003) 179–184.
[17] M.N. Avettand-Fenoel, R. Taillard, J. Dhers, J. Foct, Int. J. Refract. Met. Hard Mater. 21 (2003) 205–213.
[18] T. Zhang, Y. Wang, Y. Zhou, T. Lei, G. Song, J. Mater. Sci. 41 (2006) 7506–7508.
[19] Yu.V. Milman, A.B. Olshanskii, I.V. Gridneva, N.P. Korzhova, S.I. Chugunova, Powder Metall. Met. Ceram. 25 (7) (1986) 557–560.
[20] M. Rieth, B. Dafferner, J. Nucl. Mater. 342 (2005) 20–25.
[21] M. Rieth, A. Hoffmann, Adv. Mater. Res. 59 (2009) 101–104.
[22] Y. Zhang, A.V. Ganeev, J.T. Wang, J.Q. Liu, I.V. Alexandrov, Mater. Sci. Eng., A. 503 (2009) 37–40.
[23] H. Kurishita, S. Kobayashi, K. Nakai, T. Ogawa, A. Hasegawa, K. Abe, H. Arakawa, S. Matsuo, T. Takida, K. Takebe, M. Kawai, N. Yoshida, J. Nucl. Mater. 377 (2008) 34–40.
[24] H. Kurishita, S. Matsuso, H. Arakawa, T. Hirai, J. Linke, M. Kawai, N. Yoshida, Adv. Mater. Res. 59 (2009) 18–30.
[25] N. Nita, R. Schaeublin, M. Victoria, J. Nucl. Mater. 329–333 (2004) 953–957.
[26] Y. Chimi, A. Iwase, N. Ishikawa, M. Kobiyama, T. Inami, S. Okuda, J. Nucl. Mater. 297 (2001) 355–357.
[27] M. Rose, A.G. Balogh, H. Hahn, Nucl. Instrum. Methods Phys. Res. Sect. B 127–128 (1997) 119–122.
[28] T.D. Shen, S. Feng, M. Tang, J.A. Valdez, Y. Wang, K.E. Sickafus, Appl. Phys. Lett. 90 (26) (2007) 263115.
[29] B. Radiguet, A. Etienne, P. Pareige, X. Sauvage, R. Valiev, J. Mater. Sci. 43 (2008) 7338–7343.
[30] H. Kurishita, S. Matsuo, H. Arakawa, M. Narui, M. Yamazaki, T. Sakamoto, S. Kobayashi, K. Nakai, T. Takida, K. Takebe, M. Kawai, N. Yoshida, J. Nucl. Mater. 386–388 (2009) 579–582.
[31] M.A. Monge, M.A. Auger, T. Leguey, Y. Ortega, L. Bolzoni, E. Gordo, R. Pereja, J. Nucl. Mater. 386–388 (2009) 613–617.
[32] T. Ryu, K.S. Hwang, Y.J. Choi, H.Y. Sohn, Int. J. Refract. Met. Hard Mater. 27 (2009) 701–704.
[33] Z. Zhang, S. Wahlberg, M. Wang, M. Muhammed, Nanostruct. Mater. 12 (1999) 163–166.
[34] S. Wahlberg, I. Grenthe, M. Muhammed, Nanostruct. Mater. 9 (1997) 105–108.
[35] M. Wang, M. Muhammed, Nanostruct. Mater. 11 (1999) 1219–1229.
[36] Z. Zhang, Y. Zhang, M. Muhammed, Int. J. Refract. Met. Hard Mater. 20 (2002) 227–233.
[37] Z. Zhang, M. Muhammed, Thermochim. Acta 400 (2003) 235–245.
[38] G. Maizza, S. Grasso, Y. Sakka, T. Noda, O. Ohashi, Sci. Technol. Adv. Mater. 8 (2007) 644–654.
[39] M. Nygren, Z. Shen, Solid State Sci. 5 (2003) 125–131.
[40] Z. Shen, M. Johnsson, Z. Zhao, M. Nygren, J. Am. Ceram. Soc. 85 (8) (2002) 1921–1927.
[41] Y. Waseda, K. Hirata, M. Ohtani, High Temp. – High Press. 7 (1975) 221–226.
[42] Hk. Muller-Buschbaum, H.G.v. Schenering, Z. Anorg. Allg. Chem. 340 (1965) 232.
[43] Y. Kim, M.-H. Hong, S.H. Lee, E.-P. Kim, S. Lee, J.-W. Noh, Met. Mater. Int. 12 (3) (2006) 245–248.
[44] Y. Kim, K.H. Lee, E.-P. Kim, D.-I. Cheong, S.H. Hong, Int. J. Refract. Met. Hard Mater. 27 (5) (2009) 842–846.
[45] X. Xi, Z. Nie, J. Yang, X. Fu, W. Wang, T. Zuo, Mater. Sci. Eng., A 394 (2005) 360–365.
[46] K. Lu, L. Lu, S. Suresh, Science 324 (2009) 349–352.